Received: 10 October 2023 | Revised: 29 December 2023 | Accepted: 15 January 2024

DOI: 10.1002/nano.202300153

RESEARCH ARTICLE

Nano Select WILEY

Fractionation of flavonols and anthocyanins in winemaking residues using molecularly imprinted cellulose-synthetic hybrid particles with pyridyl active surface

Catarina P. Gomes[1] | **Rolando C. S. Dias**[1] | **Mário Rui P. F. N. Costa**[2]

[1]Centro de Investigação de Montanha (CIMO), Instituto Politécnico de Bragança, Bragança, Portugal

[2]LSRE, Faculdade de Engenharia da Universidade do Porto, Porto, Portugal

Correspondence
Rolando C. S. Dias, Centro de Investigação de Montanha (CIMO), Instituto Politécnico de Bragança, Campus de Santa, Apolónia, 5300-253 Bragança, Portugal.
Email: rdias@ipb.pt

Funding information
BacchusTech-Integrated Approach for the Valorization of Winemaking Residues, Grant/Award Number: POCI-01-0247-FEDER-069583; Competitiveness and Internationalization Operational Program, Grant/Award Number: COMPETE 2020; European Regional Development Fund; Foundation for Science and Technology; CIMO, Grant/Award Numbers: UIDB/00690/2020, UIDP/00690/2020; SusTEC, Grant/Award Number: LA/P/0007/2020; LSRE-LCM, Grant/Award Numbers: UIDB/50020/2020, UIDP/50020/2020; ALiCE, Grant/Award Number: LA/P/0045/2020

Abstract

Hybrid cellulose-synthetic particles with surface active pyridyl moieties and molecularly imprinted cavities for quercetin were prepared via atom transfer radical polymerization. The functionalization of the materials with pyridyl groups was confirmed by FTIR and the SEM micrographs of the hybrid particles demonstrate a clear surface modification compared with the pristine cellulose. Competitive sorption/desorption testing of the imprinted and non-imprinted particles with standard polyphenols show the achievement of an imprinting factor IF ~8. Moreover, it was also confirmed the high retention capability of the hybrid materials for polyphenols, due to their strong binding with the surface pyridyl moieties, even when using hydroalcoholic solvents of high ethanol content (e.g., ethanol/water 80/20 v/v). The sorption capabilities of the synthesized materials for polyphenols were explored with the fractionation of flavonols and anthocyanins in winemaking residues. High concentration and enrichment factors were achieved for high-added value compounds, namely five times for quercetin and 12 for quercetin-3-O-glucuronide with a diatomaceous earth extract and up to 4 for flavonols in a grape pomace (e.g. myricetin and quercetin glucosides). This research demonstrates de feasibility for the combination between the development of engineered materials addressing sustainability with their application to the valorization of agro-industrial wastes.

KEYWORDS

Anthocyanins, Atom transfer radical polymerization, Cellulose, Flavonols, Natural-synthetic hybrid particles, Pyridyl groups, Surface molecular imprinting, Winemaking residues

1 | INTRODUCTION

Pyridine-based polymers find special applications in science and engineering due to the particular features of the pyridyl moieties in their backbones. The physical and chemical properties of pyridine heterocycle outstand the application of this small molecule in chemical industries for a plethora of applications (pharma, food supplements, insecticides, advanced materials, etc.) while the pyridyl group excels in the correspondent macromolecular

materials (often stemming from the monomers 2-vinyl pyridine, 4-vinyl pyridine or 2-methyl-5-vinyl pyridine). In brief, many particular features of pyridine/pyridyl groups, namely as compared with benzene/benzyl groups, stem from the –N = group in these rings, namely owing to the ability of the extra electron pair that is not involved in the ring conjugation system to participate in strong H-bonding mechanisms or to bind with protons. Indeed, pyridine and the pyridyl group behave as proton acceptors, being weak bases (pKa = 5.22 for pyridine) and also as a good ligand for multiple metal ions, giving rise to complexation.[1] Actually, pyridine-based polymers are used in practice as advanced materials in a wide range of domains, including the treatment of wastewater and industrial effluents (e.g. copper, nickel, chromium and mercury adsorption), noble metals recovery (e.g., gold adsorption from aqueous solutions or uranium capture in nuclear plants), enzymes/protein adsorption, electronics (e.g. light-emitting devices, sensors and electrochemical applications), biomedicine, or even catalysis.[1–8] The sorption of phenolic contaminants with pyridine-based polymers was also considered some decades ago[9–11] and the outperformance of the pyridine-based adsorbents, namely in comparison with styrene-DVB, copolymers was observed.[1]

Notably, adsorbents with pyridyl moieties present also a strong binding with phenolic compounds in different kinds of plant extracts and are being considered for valorization of these classes of bioactive compounds.[12–18] Actually, multivalent hydrogen bonding of the phenolic groups in polyphenols (e.g. quercetin and other related flavonoids) with the pyridyl groups in the polymer networks is possible at a relatively high binding strength. Phenolic groups have a higher acidity as compared to other kinds of hydroxyls, namely the OH groups in the sugar moieties, because with the ionization of phenolic hydroxyls the negative charge and a set of the lone pair electrons in the phenoxide oxygen are delocalized by resonance to the carbons on the aromatic ring (the same is not possible with OH groups in sugars). At the end, the favorable interaction of the nucleophilic pyridyl group (weak base) with the phenolic hydroxyls (acidic groups) grounds the observed good performance of the related polymer networks for the retention of polyphenols, even at low extent of hydrophobic effects.[12–18]

Targeting of specific compounds and/or functional groups with polymers arises from the particular selection of the functional moieties in the macromolecular chains. Besides this polymer functionalization level, an additional gain for materials tailoring can be conceived through the molecular imprinting technique that ideally leads to the formation of stereospecific cavities inside a polymer network. The special features of molecularly imprinted polymers (MIPs) make these materials to perform in the separation, enrichment, and purification of plant active products and many promising developments are expected in this area for the next years.[19–21]

The present work fits in this line of thought and tries to join in the same material three main features: i) functionalization with pyridyl groups, (ii) molecular imprinting with quercetin, iii) core–shell architecture for cellulose-synthetic hybrid particles.

The latter characteristic of the materials explores the creation of an active surface with pyridyl groups and molecular imprinted cavities in cellulose-synthetic hybrid particles. This architecture is achieved through atom transfer radical polymerization (ATRP), involving cellulose particles acting as a macroinitiator (an ATRP initiator is previously immobilized at cellulose particles surface), the functional monomer 4-vinylpyridine, a crosslinker for network formation and quercetin as imprinting template. The addressing of hybrid materials with cellulose and natural polysaccharides in general is being actively considered in polymer science and industry in view of improvement of sustainability, e.g. in adsorption,[22] surface modification,[23] electronics[24] including actuators,[25] or even CO_2 capture,[26] among many other routes and applications involving cellulose adaptation.[27–29] Our approach, with inclusion of cellulose, also attempts to fit on the ongoing research lines pursuing the "greenification" of MIP materials for advanced applications.[30,31] Overall, the particles developed in this work enclose a pyridyl active shell surface, enhancing mass transfer rates and binding site accessibility (important issues in sorption/desorption phenomena), while the core is made of cellulose. At the end, a substantial weight fraction of the hybrid particles is a natural material (cellulose core) while the relevant synthetic pyridyl active shell, aimed to target polyphenols, has a minor contribution for material weight composition.

The exploitation of agro-industry generated waste and by-products to obtain high added-value products, namely drugs, nutraceuticals, cosmeceuticals and platform chemicals in general is part of the United Nations 2030 Agenda for Sustainable Development. In this context, the developed materials are here applied to the valorization of winemaking residues through the targeting of the flavonols and anthocyanins there contained, thus endeavoring contributing for sustainability and circular bio-economy. Actually, it is well known that grapevine and winemaking residues are a valuable feedstock for biorefinery because contain relevant amounts of cellulose, hemicellulose and lignin that can be used to produce biofuels (e.g. bioethanol, biobutanol) and many platform chemicals.[32] These residues also include a plethora of phenolic compounds, such as flavonoids, phenolic acids,

stilbenes and macromolecules (e.g. tannins) that are suitable for economical exploitation in pharmaceutical, nutraceutical and cosmetic industries, after their purification. According to statistics of 2019, a global grape production of 77.1 million tones was observed, with 57% of this amount applied to wine production (29 million tons of wine estimated to be produced in 2018). Vineshoots (6.9–13.8 million tons produced per year), stalks (1.3–1.8 million tons per year), grape pomace (5.7–8.8 million tons per year) and wine lees (0.7–2.6 million tons per year) are the major classes of grapevine and winemaing residues being generated by this agricultural/industrial activity.[32] The approaches nowadays being considered for the valorization of polyphenols in winemaking residues aim at stable and economically feasible processes. Issues related with the variability of the biomass geographical origin, collection season and grape varieties, etc. motivate the use of efficient extraction and purification methods for polyphenols, allowing their steady supply. A complex mixture of compounds is inevitably obtained when the winemaking residues are extracted, independently of the method used in the range of techniques often considered (hydroalcoholic maceration, ultrasounds assisted, supercritical fluids, etc.). In this context, it is mandatory the development of sustainable separation and purification methods to get individual polyphenol molecules or mixtures suitable for practical applications in the downstream industries (mainly the pharma, feed, food and cosmetic industries). A lower energy consumption, cyclability, preservation of temperature-sensitive compounds, operational flexibility, amenability to intensification, and industrial scalability make the purification of polyphenols by sorption/desorption highly competitive in comparison with the alternative crystallization or membrane filtration approaches.

Specifically, in this work, the residual diatomaceous earth used for wine filtration and grape pomace resulting from the vinification process are considered as feedstocks to get the enrichment of high added value compounds through sorption/desorption with the developed particles. Winemaking industry generate large amounts of residual diatomaceous earth (an amorphous silica network), used for wine filtration, which is, as well, a rich and currently underexploited source of phenolic compounds.[16] On the other hand, grape pomace is the major by product resulting from the grapes pressing (stalks/stems are in general previously separated in the destemming step) and is estimated to constitute 15–30% (depending on grape varieties, etc.) of the total weight for the bunch. Grape pomace is mainly composed of processed skins and seeds. Besides stalks/stems (5%–7%) and grape pomace, winemaking also generates lees (2%–6%) that result from the fermentation and sedimentation steps, thus containing dead yeast cells.[32,33] Grape pomace can be used for ethanol production, composting, production of fertilizers or as livestock feed but is often disposed of in landfills with important environmental impacts.[32] However, the great potential of grape pomace as lignocellulosic biomass and/or to produce extracts rich in phenolic compounds (e.g. phenolic acids, anthocyanins and flavonols) is gaining room via recent studies in the framework of circular bio-economy.[32] In a simple estimate, considering the recent years annual production of 60–80 million tons of grapes (with c.a. 60% used for winemaking) and estimating the generation of 130 to 200 kg of grape pomace per ton of grapes,[32] a rough range of 5–10 million tons of grape pomace is available per year as biomass for valorization.

2 | RESULTS AND DISCUSSION

2.1 | Materials design and characterization

Figure 1 depicts the reaction steps considered for the synthesis of molecularly imprinted cellulose-synthetic hybrid particles with pyridyl active surface. In brief, the first step deals with the immobilization of α-bromoisobutyryl bromide (BIBB) in microcrystalline cellulose (MCC), as schematized in Figure 1A, with generation of an ATRP macroinitiator MCC-Br particles. Afterwards, as schematized in Figure 1B, a thin synthetic shell with imprinted cavities is created at the surface of the cellulose particles, via ATRP polymerization. This second reaction step involves the macroinitiator MCC-Br particles, the functional monomer 4VP, the crosslinker EGDMA and the template quercetin, with the presence of the pair CuBr/PMDETA for the ATRP activation/deactivation mechanism. Non-imprinted material synthesis follows the same procedure with the absence of the quercetin template (see experimental details in ref. [17]). Concerning cellulose modification, this approach follows the reported approaches for synthetic surface grafting using ATRP.[34–36] Hybrid particles generated by surface initiated ATRP (SI-ATRP) can be conceived with different kinds of core materials such as silica, metal particles or cellulose.[37–39] This research considered cellulose for this purpose due to its abundance, biodegradability, biocompatibility and the framework of both, the developed adsorbents and application, in the agro-industrial field. Furthermore, our aim is the fabrication of molecularly imprinted cavities with quercetin as template, and for this purpose, this polyphenol was included in the second step reaction mixture. A thin enough synthetic layer is sought in this technique, to enhance mass transfer and binding site accessibility, and therefore the proper

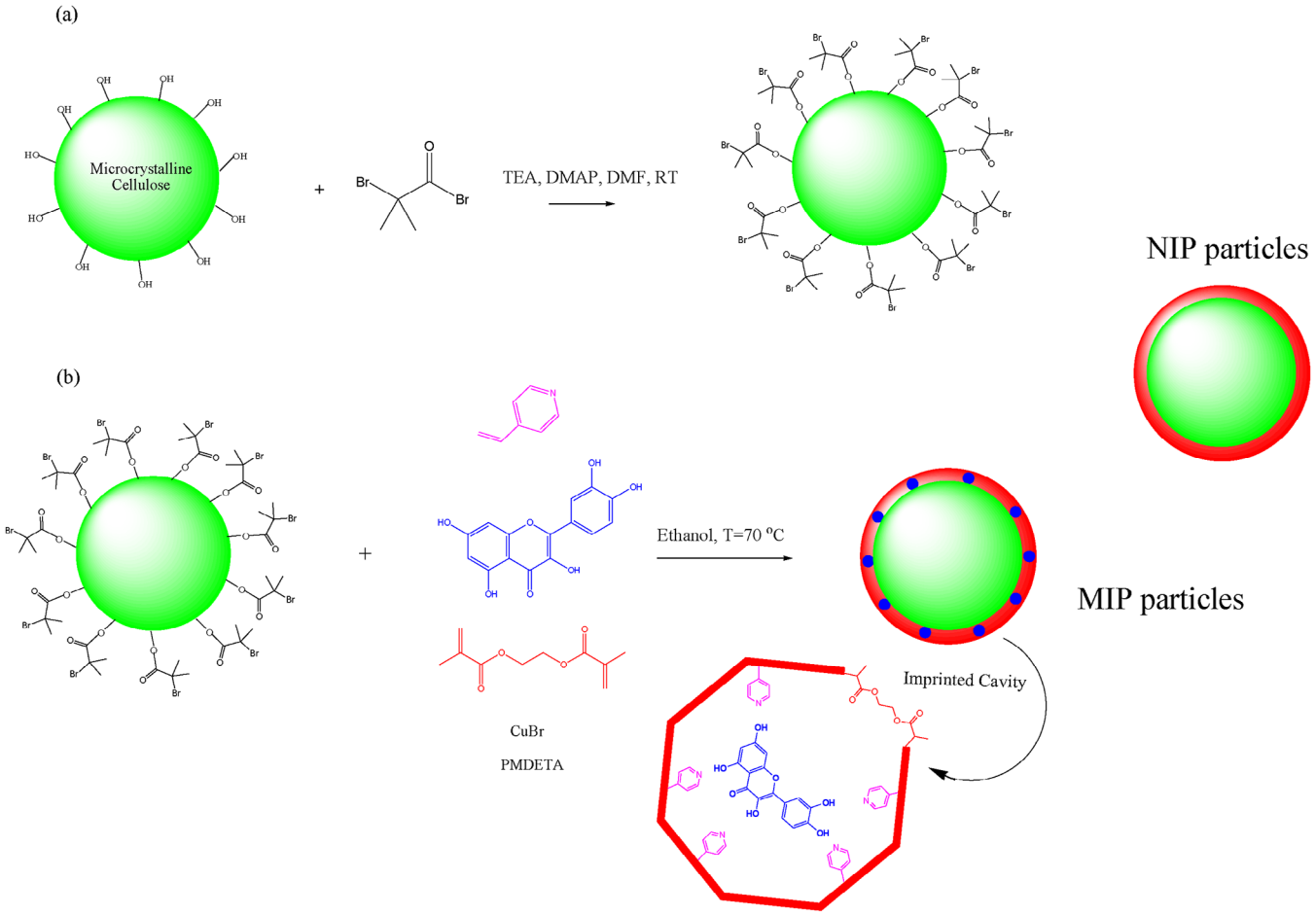

FIGURE 1 Depiction of the synthesis procedure considered for the development of surface molecularly imprinted cellulose-synthetic hybrid particles via ATRP. A, Immobilization of α-bromoisobutyryl bromide in pristine microcrystalline cellulose (MCC) to generate ATRP macroinitiator particles (MCC-Br). B, Grafting of a crosslinked-imprinted shell in the particles surface considering ATRP of co-monomers 4VP/EGDMA in the presence of quercetin.[17] The synthesis of non-imprinted polymer (NIP) particles (absence of the template molecule) is also depicted.

reaction conditions should be addressed. It was previously observed[17] the formation of cellulose-synthetic hybrid particles with a 14 wt% 4VP/EGDMA shell, when working with ethanol as solvent in the second reaction step (Figure 1B) and [4VP] = 87.4, [EGDMA] = 17.4, [Quercetin] = 6.5, [CuBr] = 1.9, [PMDETA] = 1.9, [Ethanol] = 16898 mM, [MCC-Br] = 5.15 mg mL^{-1} (see ref. [17] for other synthesis conditions tested). Moreover, it was demonstrated that these specific particles, obtained through a solid/liquid heterogeneous ATRP process in ethanol, preserve a final size suitable for their application as adsorbent[17] and therefore will be here also used. Other approaches are being scouted in the literature for the synthesis of hybrid cellulose-synthetic particles with molecular imprinting of polyphenols considering the free radical route instead of the controlled polymerization here explored. For instance, porous cellulose-based molecular imprinted particles for enrichment of resveratrol were prepared through the silanization of porous cellulose particles with 3-methacryloxypropyltrimethoxysilane followed by the formation of the synthetic part by reacting the C = C in the cellulose in the presence of EGDMA, 4VP and resveratrol (the template for imprinting) with AIBN as initiator.[40] A potential advantage of the route here considered is the improved tailoring of the synthetic shell formation achieved with controlled radical polymerization as compared to the FRP mechanisms.

The FTIR (Fourier-transform infrared spectroscopy) analysis of the intermediate products (MCC-Br particles) and final cellulose-synthetic hybrid materials highlight the achievements on the native cellulose modification and creation adsorbents with a pyridyl active surface. In brief (see Figure S1 in the Supplementary Material and ref. [17]): i) a new peak at 1740 cm^{-1} is observed in MCC-Br as a consequence of the stretching of the carbonyl group (-C = O) resulting from the reaction between OH groups in cellulose and BIBB, ii) The presence of EGDMA in the final cellulose-synthetic hybrid particle is confirmed

through the vibrational assignments at 1720 and 1130 cm^{-1} (C = O and C–O groups, respectively), (iii) the functionalization of the final materials with pyridyl groups is demonstrated via the characteristic peaks at 1600 cm^{-1} (C = C pyridyl), 1418 cm^{-1} (C = N), 820 cm^{-1} and 755 cm^{-1} (both correspond to the C–H bending in the pyridine ring). A thin enough imprinted shell is here attempted in order to enhance binding site accessibility and mass transfer. For that, a low concentration of the monomers 4VP and EGDMA was used, and therefore, a weaker FTIR response of 4VP characteristic groups is expected (see refs. [12–18] dealing with different amounts of 4VP in the polymerization recipes).

Notably, the SEM analysis of the native MCC particles and of the molecularly imprinted and non-imprinted cellulose-synthetic hybrid materials highlight the modification of the surface achieve through the incorporation of the synthetic shell. Figure 2 presents relevant SEM micrographs that put into evidence these outcomes. Figure 2A and B shows the morphology of the pristine MCC particles used in this work (microcrystalline cellulose powder, 20 μm, cotton linters, as designed by the supplier) with a wide dispersion in size (mostly in the range 5 to 50 μm) and the irregular format is discernible for these cotton linters. Figure 2C,D and E,F shows similar micrographs for the NIP (non-imprinted polymer) and MIP cellulose-synthetic hybrid particles, respectively. Overall, a global slight increase of the particle size seems to occur as a consequence of the grafting of the synthetic layer (characteristic size < 50 μm), both for NIP and MIP particles (see comparison of Figure 2C and E with Figure 2A). Remarkably, figures D and F, in comparison with figure B, clearly evidence the surface modification achieved for the native MCC particles through the creation of a 4VP/EGDMA synthetic layer, both in NIP and MIP developed materials. Pictures added in the SEM micrographs for the surface of cellulose, NIP and MIP highlight these differences in articulation with the schemes presented in Figure 1.

Overall, the nitrogen adsorption/desorption measurements with the native MCC particles and the cellulose-synthetic hybrid materials show very similar low specific surface area (9.3 m^2 g^{-1} for the MIP particles and 8.6 m^2 g^{-1} for the native MCC), which is consistent with previous observations for totally synthetic 4VP/EGDMA particles (2–4 m^2 g^{-1}) indicating a low porogenic effect for such polymer networks formation.[15] Despite these low values for specific surface area (e.g. 135 m^2 g^{-1} estimated for the commercial resin DAX8) very high capabilities of the 4VP/EGDMA materials for adsorption of polyphenols are found as compared with several kinds of alternative adsorbents.[12–18] The functionalization of these materials with pyridyl groups is at the source of these outcomes, as discussed in the introduction section and also explored in the forthcoming analysis.

2.2 | Competitive sorption/desorption in imprinted and non-imprinted particles with standard polyphenols

Having above put into evidence the surface modification achieved both for imprinted and non-imprinted particles, as compared to the native MCC, the effects of molecular imprinting were assessed through competitive sorption/desorption runs in the MIP and NIP hybrid materials. For that purpose, a mixture of the standard phenolic compounds ferulic acid, rutin and quercetin in ethanol/water 80/20 was loaded to the particles in SPE (solid-phase extraction) columns, followed by the washing (ethanol/water 80/20) and elution (methanol/acetic acid 90/10) steps. The composition of the column outlet for these three steps was determined by HPLC-DAD. The selection of ferulic acid, rutin and quercetin was motived by their representation of three major classes of phenolic compounds found in winemaking residues, namely the phenolic acids, glycosylated flavonoids and aglycone flavonoids, respectively. Additionally, quercetin was used as an imprinting template and therefore these competitive sorption/desorption runs with NIP/MIP particles can provide insights on the potential benefits of molecular imprinting. The selection of quercetin as imprinting template was driven by its reference structure for many flavonoid molecules, large availability (present in many different kinds of plants and related residues) and lower price. Actually, quercetin is a less expensive molecule and consequently can be used as surrogate for flavonoids imprinting.

Figure 3 presents results for the HPLC-DAD analyses of the solutions collected at MIP and NIP SPE column outlet after the competitive loading step of the mixture of polyphenols. A clear high retention of quercetin in the quercetin-MIP (ca 62.1%) is observed as compared with the NIP (ca 7.4%) indicating a favorable impact of molecular imprinting for the retention of the template molecule under competitive sorption conditions. Taking in consideration the retention amounts determined by HPLC-DAD an imprinting factor IF = 8 is estimated under these competitive sorption conditions. Note that for non-competitive sorption, an imprinting factor IF = 2.6 was estimated for these same particles.[17] In reference[17] were also presented results for individual sorption/desorption assays with rutin, oleuropein and vanillic acid and demonstrated the relevant impact of NIP/MIP functionalization with pyridyl groups to enhance adsorption of polyphenols comparatively to the native cellulose.

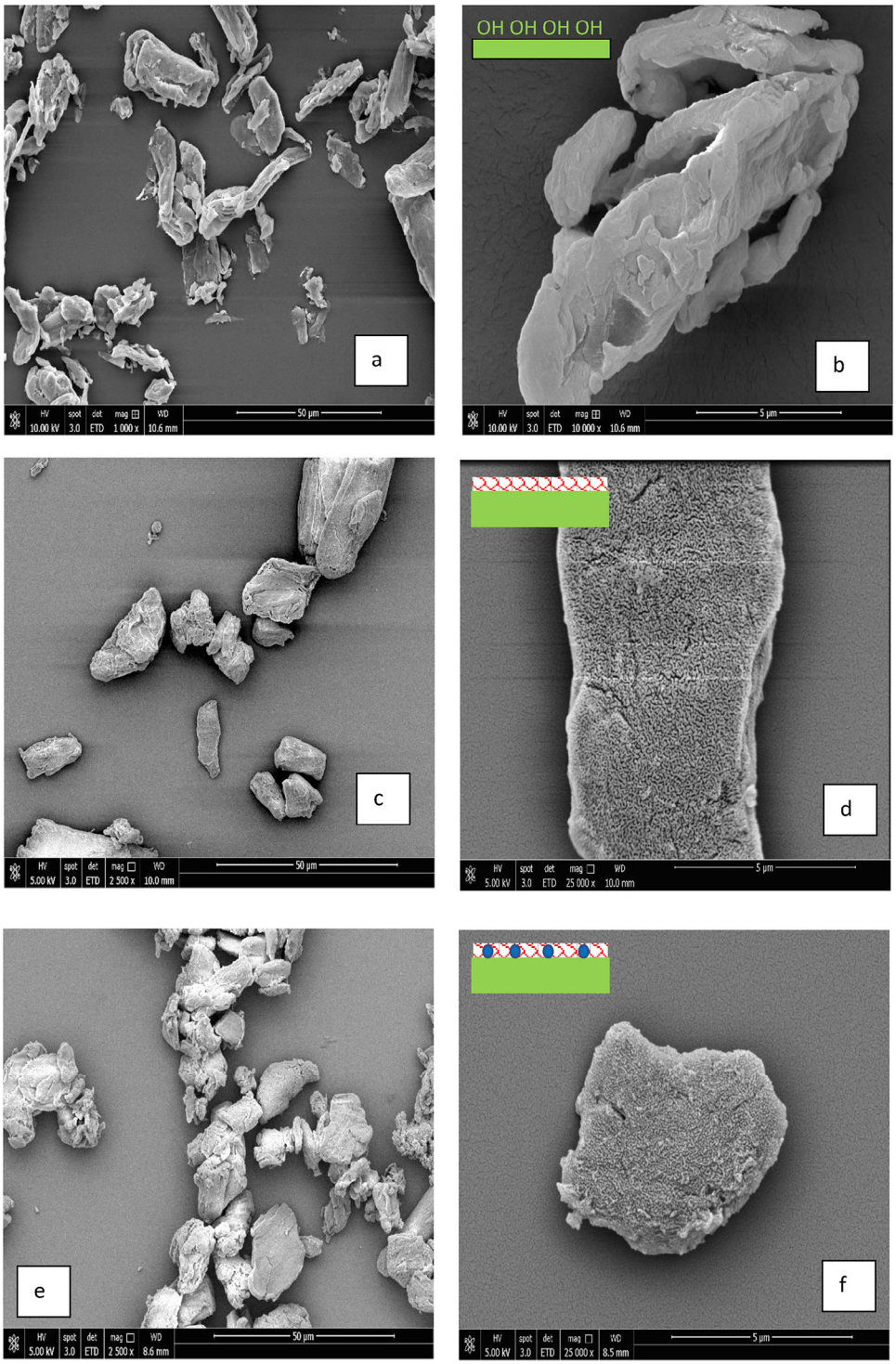

FIGURE 2 SEM images for the pristine cellulose particles (A and B), NIP hybrid cellulose-synthetic particles with pyridyl active surface (C and D) and MIP hybrid cellulose-synthetic particles with pyridyl active surface (E and F).

Additional insights on the strength of the competitive binding of the three polyphenols in MIP and NIP particles are obtained analyzing the washing and elution, steps as presented in the Supplementary Material for the correspondent HPLC-DAD analyses (Figures S2 and S3) and summarized in Figure 4. A very strong binding of quercetin in the MIP is observed via the analysis of the high amounts of this molecule retained even after washing and elution of the particles. In opposition, rutin and ferulic acid are totally removed from the particles along the washing and elution steps, indicating a much lower binding affinity. These outcomes clearly demonstrate the

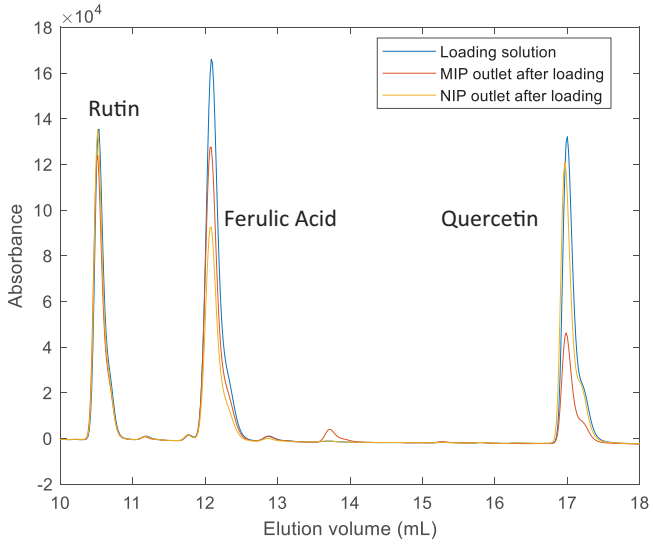

FIGURE 3 HPLC-DAD analyses for the solutions collected at MIP and NIP SPE columns outlet after the loading step. Competitive sorption/desorption assessment using a ferulic acid/rutin/quercetin solution in ethanol/water 80/20 with concentration 0.1×10^{-3} M for each compound, 2.5 mL of volume of liquid phase and 25 mg of adsorbent in the SPE cartridges. UV measurements at 280 nm are here presented.

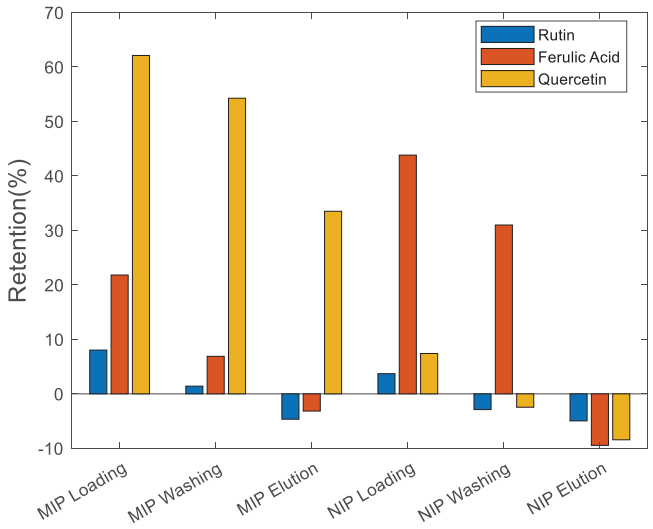

FIGURE 4 Fraction of the initial amount of standard compound's rutin, ferulic acid and quercetin retained in MIP and the NIP hybrid particles after the competitive loading, washing, and elution steps in SPE, according to the conditions specified in Figure 3. The retained amounts were estimated through the HPLC-DAD analysis of the samples collected at column outlet.

achievements obtained with molecular imprinting through the formation of binding sites enhancing the retention of quercetin.

Interestingly, with the NIP particles, under the same competitive conditions, a stronger binding is observed for ferulic acid as compared with rutin and even quercetin (see Figures 3 and 4 and also S2 and S3 in the Supplementary Material). To help with the interpretation of such results, in Figure 5, it is presented a simple sketch for the plausible interactions of the three standard polyphenols with the imprinted pyridyl active surface giving foundations for their different adsorption. For quercetin, a multivalent hydrogen bonding of the phenolic groups with the pyridyl moieties, enhanced due to stereospecificity for MIP cavities, is possible as represented in Figure 5A. A lower number of interactions of such kind is expected with rutin or ferulic acid. Note that, phenolic groups have an increased acidity as compared to -OH in the sugar moieties (see rutin molecular structure in Figure 5). Actually, with ionization of phenolic hydroxyls the negative charge and a set of the lone pair electrons in the phenoxide oxygen are delocalized by resonance to the carbons on the aromatic ring. Thereafter, the nucleophilic pyridyl group (a weak base) has a stronger binding with phenolic hydroxyls as compared with the -OH groups in the sugar rings of rutin (charge delocalization not possible). Also, for rutin, steric hinderance is possible for binding due to the higher size of the molecule. These issues explain the low binding capacity observed for rutin, both with the MIP and NIP particles.

For ferulic acid, in spite of the low number of phenolic hydroxyls (Figure 5C), the higher acidity of the carboxylic group (pK_a = 4.61 for ferulic acid) should contribute to increase the interaction with the weakly basic pyridyl moieties (pKa = 5.22 for pyridine base) in the active surface, both in MIP and NIP, in spite of the complex ionization effects with aqueous solvent mixtures. This explains the high retention for ferulic acid observed with the NIP and the low displacement observed for this molecule during the washing step with ethanol/water 80/20 (see, e.g., Figure 4). However, in the elution step with methanol/acetic acid 90/10, the ferulic acid is totally desorbed (Figure 4), and this is enhanced by the presence of acetic acid and concomitant competition for binding with the basic pyridyl moieties. Note that the same situation was not observed for elution of quercetin in the MIP, giving support for the importance of the imprinted cavities for the very high binding strength of this molecule in this material. These imprinting cavities should also play a central role with quercetin preferential competitive sorption in the MIP compared to the favorable retention of ferulic acid in the NIP under similar competitive conditions.

Hydrophobic effects and competitive interaction of the pyridyl groups with solvent molecules (water, ethanol, acetic acid, etc.) are additional issues influencing the sorption/desorption processes. A "nonideal" interferent solvent for MIPs performance is here being used

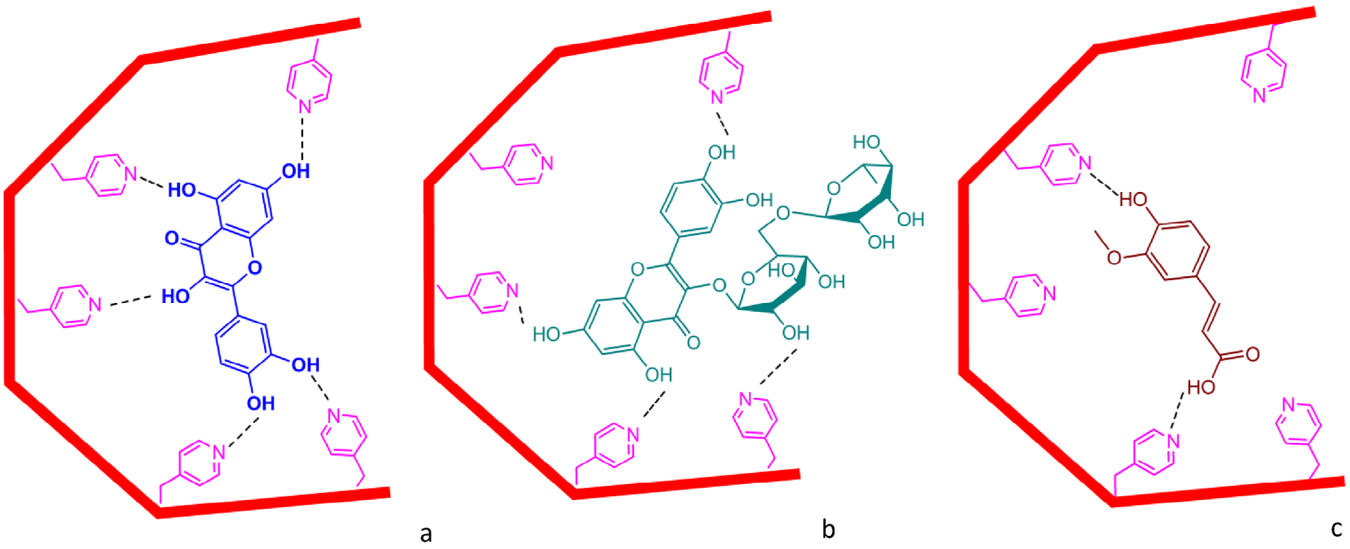

FIGURE 5 Simple sketch for some plausible intermolecular interactions of (A) quercetin, (B) rutin, and (C) ferulic acid with the pyridyl active surface of the molecularly imprinted cellulose-synthetic hybrid particles synthesized in this work. A multivalent hydrogen bonding of the phenolic groups in quercetin with the pyridyl groups in the surface is possible. Lower number of pyridyl-phenolic hydrogen bonding interactions are expected for rutin and ferulic acid and steric hinderance is possible for rutin. Hydrophobic effects, competitive interaction of pyridyl groups with solvent molecules are other issues influencing solute sorption/desorption processes. In spite of the expected effect of the stereospecificity of the surface imprinted cavities in the MIP particles, similar interactions are possible with the surface of the non-imprinted particles (NIP).

(ethanol/water mixtures) to avoid other toxic and less biocompatible solvents (e.g. acetonitrile).

The knowledge acquired with the competitive sorption analysis above presented is applied below for the enrichment of polyphenols in winemaking residues, namely using the special features of the developed MIP particles to target flavonoids and related kinds of polyphenols.

2.3 | Application with diatomaceous earth extracts

Here it is addressed the performance of the developed molecularly imprinted cellulose-synthetic hybrid particles with pyridyl active surface as adsorbent for the fractionation and enrichment of flavonoids in residual diatomaceous earth. Within this purpose, a hydroalcoholic extract of this material was considered as polyphenol feedstock (diatomaceous earth is used in winemaking for wine filtration and often discarded after saturation). Industrial and analytical applications already consider sorption/desorption processes in purification steps for a long time and their use with plant extracts and effluents from agro-industrial activities is also well known.[41] The adsorbents play a central role in the efficiency of such processes, namely concerning specificity/selectivity, retention capacity and easiness for their regeneration. Many synthetic polymer networks (e.g. the Amberlite, Supelite and Reillex resins) excel in such kind of applications due to the possibility for their tailoring besides the often-observed durability and stability (e.g. as compared with lignocellulosic/polysaccharide, activated carbon or silica adsorbents). An overview for different kinds of adsorbents with practical use in the valorization of agro-industrial residues, namely through the concentration of polyphenols is presented in reference[41] and recent specific cases involving sorption/desorption for the valorization od winemaking residues can be found in refs. [42, 43] and refs. therein.

Figure 6 presents the phenolic profile of this extract, obtained through HPLC-DAD analysis, and a rich composition in such kinds of compounds is observed. Among the plethora of different molecules detected, evidencing the complexity of these extracts, relevant flavonoid compounds can be identified, namely myricetin-O-hexoside (peak 13), quercetin-O-hexuronoside (14), myricetin (18), quercetin (21) and kaempferol (24). In the supplementary material, additional information is presented helping with chemical species identification in these chromatograms (Figures S4–S8), namely concerning the ones close to the analytic system peak (peak 1 in Figure 6), such as gallic acid and other phenolic acids (peak 3 and subsequent peaks up to ~ 8 minutes elution time) as well as anthocyanins (see also de next section). Detailed information on the identification of phenolic compounds in the winemaking residues extracts here considered can be found in refs.

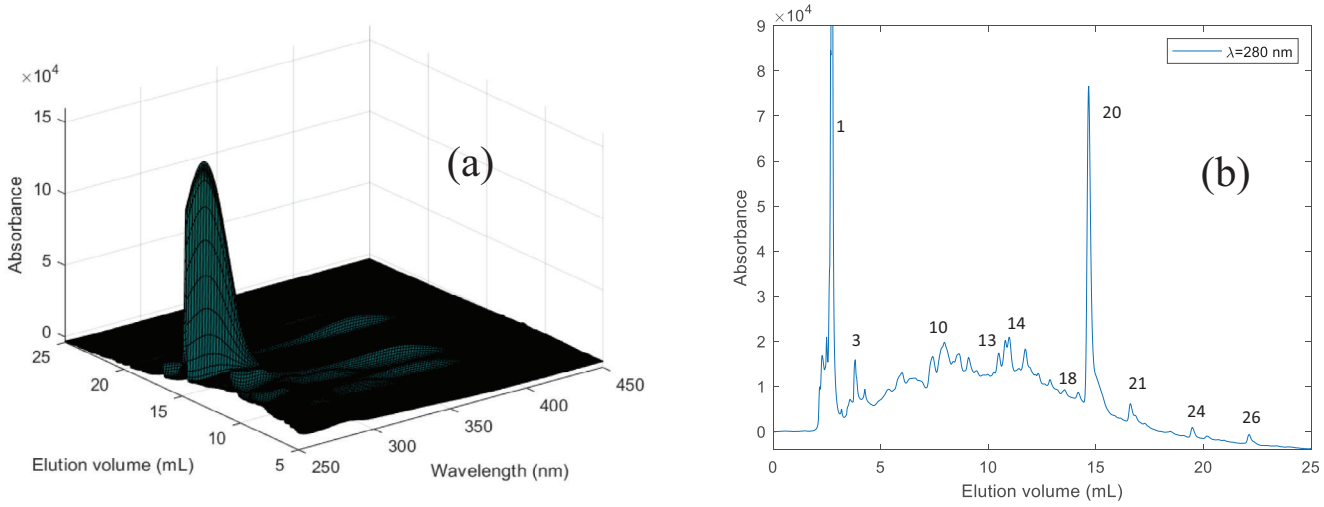

FIGURE 6 A, 3D HPLC-DAD chromatogram and (B) correspondent 2D view at 280 nm for a diatomaceous earth extract used in this work. The following relevant identification for flavonol compounds in the extract is possible: (13) myricetin-O-hexoside, (14) quercetin-O-hexuronoside, (18) myricetin, (21) quercetin, (24) kaempferol.

[16, 44]. These previous works allow to conclude that peak 20 in Figure 6 is not relative to a polyphenol molecule but another compound used during the vinification process.

Pyridyl groups have a strong binding towards phenolic compounds, as above discussed and demonstrated, even when hydroalcoholic solvents with low water content are used (e.g. ethanol/water mixtures with volume fraction of ethanol > 50 %). This is especially appealing with the processing of plant extracts containing polyphenols because allows working with high concentration (avoiding precipitation issues of such complex mixtures in water-rich solvents) and preserving a high retention in the sorption step. Having in mind the industrial application, the volume to be processed decreases (lowering energy costs with pumping) with enhancement of process intensification and sustainability.

These features were previously demonstrated with other 4VP-based adsorbents and are here explored with the hybrid cellulose-4VP MIPs for the fractionation of diatomaceous earth and grape pomace contained polyphenols. An example for the ability to make the fractionation of such polyphenol mixtures is presented in Figure 7. In this case study, the particles were previously loaded at $T = 15°C$ using a diatomaceous earth extract (Figure 6) in EtOH/water 80/20 and $C = 3.75$ mg mL^{-1}. A low temperature was considered in this run aiming at to further enhance the adsorption of phenolic compounds, namely through H-bonding interactions with the adsorbent functional groups. After that, the desorption process includes the increase of the temperature to 45°C and the percolation through the column of a sequence of solvents, starting with water, and going towards the increase of ethanol content, up to a final stage with methanol/acetic acid 90/10. This solvent-gradient process is considered to produce fractions with different polyphenols composition, exploring the variable strength of their binding with the surface of the adsorbent containing active pyridyl groups, similarly to that above demonstrated with the mixture of rutin, ferulic acid and quercetin. A first important outcome that can be observed in Figure 7 is the elimination in this fraction of the nonpolyphenol compound in the diatomaceous earth extract (peak 20 in Figure 6). Notably, results in Figure 7 also demonstrate the production of a fraction in ethanol/water 80/20 highly enriched in flavonols, namely quercetin (peak 21 in Figure 6) and quercetin-O-hexuronoside (peak 14 in Figure 6). The designation quercetin-O-hexuronoside is considered for identification because quercetin-3-glucuronide and quercetin-3-galacturonide are both possible via the LC-MS analysis.[44] However, the presence of quercetin-3-glucuronide in plant extracts, namely in vine and winemaking residues is well documented[45] and therefore is the most plausible identification for peak 14. Figure 8 presents a 3D view for the HPLC-DAD analysis of the same fraction giving further insights on the fractionation and enrichment achieved. Actually, the comparison between Figure 6 (the starting diatomaceous earth extract) and Figures 7 and 8 clearly demonstrates the good performance of the particles developed for enrichment and fractionation of polyphenols. Considering the chromatogram areas at 280 nm, enrichment factors of 5 and 10 are estimated for quercetin and quercetin-O-hexuronoside, respectively, in this fraction comparatively to the initial extract.

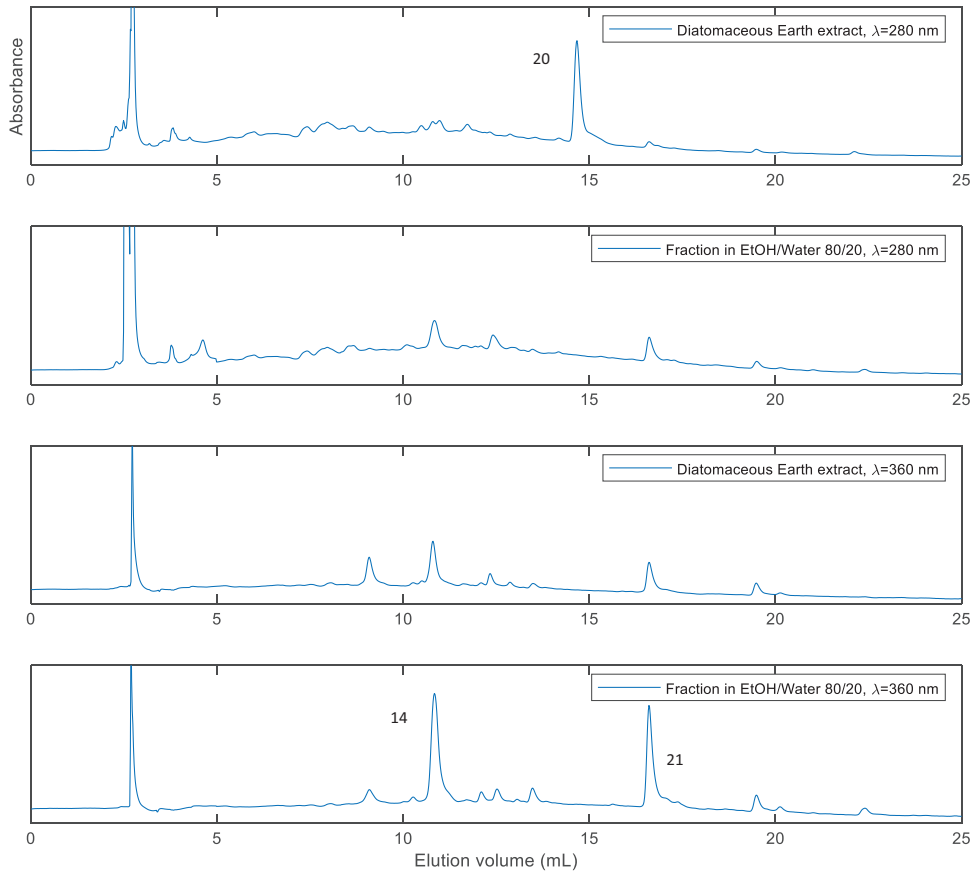

FIGURE 7 HPLC-DAD analyses for the diatomaceous earth extract and a fraction desorbed from the pyridyl active MIP hybrid particles at $T = 45°C$ with EtOH/water 80/20 as eluent. The previous sorption step was made at $T = 15°C$ using a diatomaceous earth extract in EtOH/water 80/20 and $C = 3.75$ mg mL^{-1}. The wavelengths $\lambda = 280$ and 360 nm were selected (see insets) to highlight the enrichment of flavonols in this fraction.

Figures 9 and 10 present a similar analysis for a fraction desorbed with methanol/acetic acid 90/10. Note again the important outcome related with the elimination of the nonphenolic compound correspondent to peak 20 in the produced fraction. Moreover, a huge purification and concentration effect is observed in this fraction for quercetin-O-hexuronoside (peak 14) as compared with the initial fraction. This achievement becomes clear through comparison of Figures 6, 9, and 10. Considering the chromatogram areas at 280 nm, the enrichment factor of 12 is estimated for quercetin-O-hexuronoside in this fraction comparatively to the initial extract. The extra acidic group in quercetin-O-hexuronoside (quercetin-3-glucuronide) and its higher binding strength with the basic pyridyl groups at the adsorbent surface should ground this particular separation and concentration outcome. Globally, a very high binding effect seems to be observed for this compound due the multiple interaction points with pyridyl moieties, namely the phenolic -OHs and the extra -COOH in the -glucuronide group (see Section 2.2).

2.4 | Application with grape pomace extracts

Several studies showed the rich phenolic profile of the grape pomace biomass, including phenolic acids anthocyanins and many flavonols (see, e.g.,[44] and references therein). It is well known that many of these phenolic compounds present important antioxidant and anti-inflammatory properties, able to alleviate neurodegenerative and cardiovascular diseases, thus making them very useful in the pharmaceutical, cosmetic and food industries.[44] Often, the classification of phenolic compounds considers flavonoids as a specific major class that can be subdivided into subgroups considering a three-ring structure as reference (see, e.g., the quercetin structure in Figure 5A) and analyzing the linkages relatively to the ring containing the -O- group and the degree of unsaturation and oxidation of this same ring.[46,47] When the simple linkage of other phenolic ring to that containing the -O- group occurs in position 2 a set of subgroups

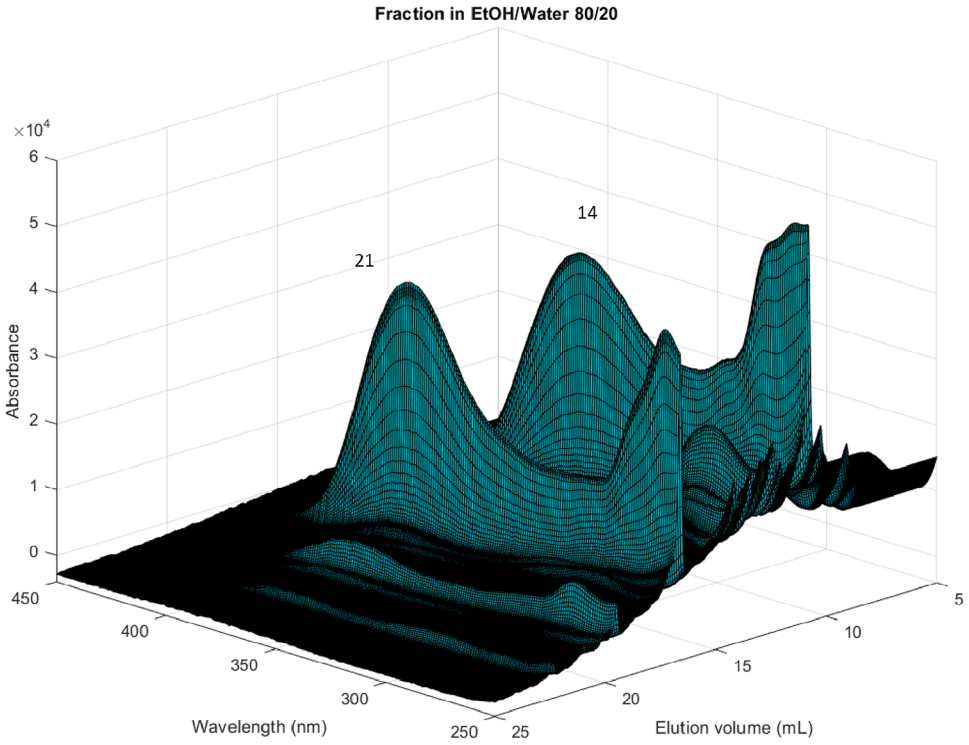

FIGURE 8 3D view for the HPLC-DAD analysis for the fraction desorbed from the pyridyl active MIP hybrid particles at $T = 45°C$ with EtOH/water 80/20 as eluent. The previous sorption step was made at $T = 15°C$ using a diatomaceous earth extract in EtOH/water 80/20 and $C = 3.75$ mg mL^{-1}. The huge enrichment with the flavonols kaempferol, quercetin and quercetin-o-hexuronoside achieved in this fraction is here highlighted.

of compounds is identified, namely flavones, flavonols (see quercetin structure), flavanones, flavanonols, flavanols (catechins), anthocyanins and chalcones.[46] It was demonstrated that, among the phenolic compounds found in grape pomace, two flavonoid classes are predominant, namely the flavonols and the anthocyanins. The aglycones quercetin, myricetin or kaempeferol and the related glycosylated analogues (rutin, myricetin-O-hexoside, quercetin-O-hexuronoside, etc.) are documented to be present in grape pomace. On the other hand, anthocyanins are glycosylated counterparts of anthocyanidins, belonging also to the flavonoid family, that are widely found in grapes, wine and winemaking residues/subproducts. The anthocyanidin malvidin and the related anthocyanin malvidin 3-O-glucoside (also named oenin), delphinidin/delphinidin 3-glucoside (myrtillin), peonidin/peonidin 3-glucoside are pairs anthocyanidin/anthocyanin with high relevance in different kinds of grape and wine varieties (e.g. defining the red, bluish, purple, etc. tonality of wine). Note that many other glycosylated counterparts of anthocyanidins are found in nature,[48] namely in grapes and wine (e.g. malvidin, delphinidin, peonidin −3,5-O-diglucosides or the -arabinose, -galactose, -rhamnose, -xylose related anthocyanins). Besides other applications, anthocyanins (synthesized by plants via the flavonoid pathway[49]) can be used as natural dyes. Their colors depend on the pH and on the methylation/acylation at the hydroxyl groups belonging to the constituent phenolic rings.[46] Actually, the equilibrium between different molecular structures (e.g. flavylium cation and quinoidal bases), explains the shift between colors observed in practice (e.g. red for the flavylium cation and blue for the quinoidal base, as observed with cyanidin-3-glucoside[50]).

Such a complex mixture of phenolic compounds in grape pomace, namely concerning the contained flavonols and anthocyanins subclasses of flavonoids, is illustrated in Figure 11 below for the extract of this biomass here considered. Our aim is to demonstrate the usefulness of the developed hybrid particles for the fractionation of these families of molecules. In Figure 12 are presented results for the fractionation of a grape pomace extract attained with the hybrid MIP particles and using a similar process to that above described with the diatomaceous earth extract. At a first stage the particles were loaded at $T = 15°C$ using an extract in EtOH/water 54/46 and $C = 1.1$ mg mL^{-1}. After that, the desorption process included the increase of the temperature to 45°C and the running of a solvent-gradient process, starting with water, afterwards increasing the ethanol content in hydroalcoholic mixtures, up to a final stage with methanol/acetic acid

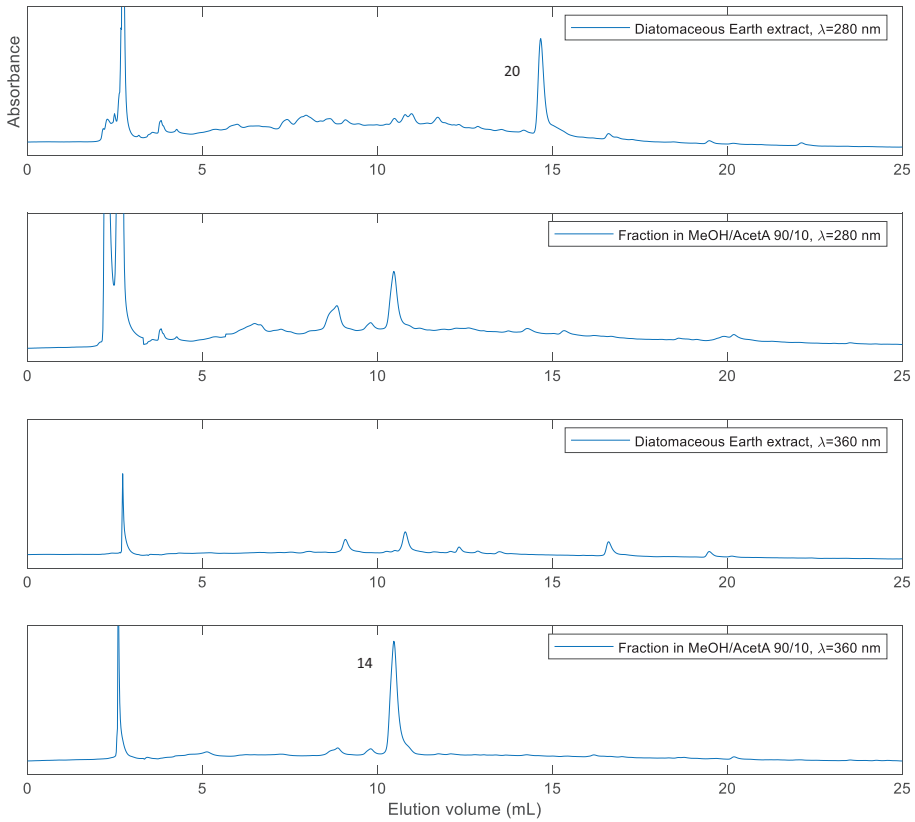

FIGURE 9 HPLC-DAD analyses for the diatomaceous earth extract and a fraction desorbed from the pyridyl active MIP hybrid particles at $T = 45°C$ with MeOH/AcetA 90/10 as eluent. The previous sorption step was made at $T = 15°C$ using a diatomaceous earth extract in EtOH/water 80/20 and $C = 3.75$ mg mL^{-1}. The wavelengths $\lambda = 280$ and 360 nm were selected (see insets) to highlight the enrichment of flavonols in this fraction.

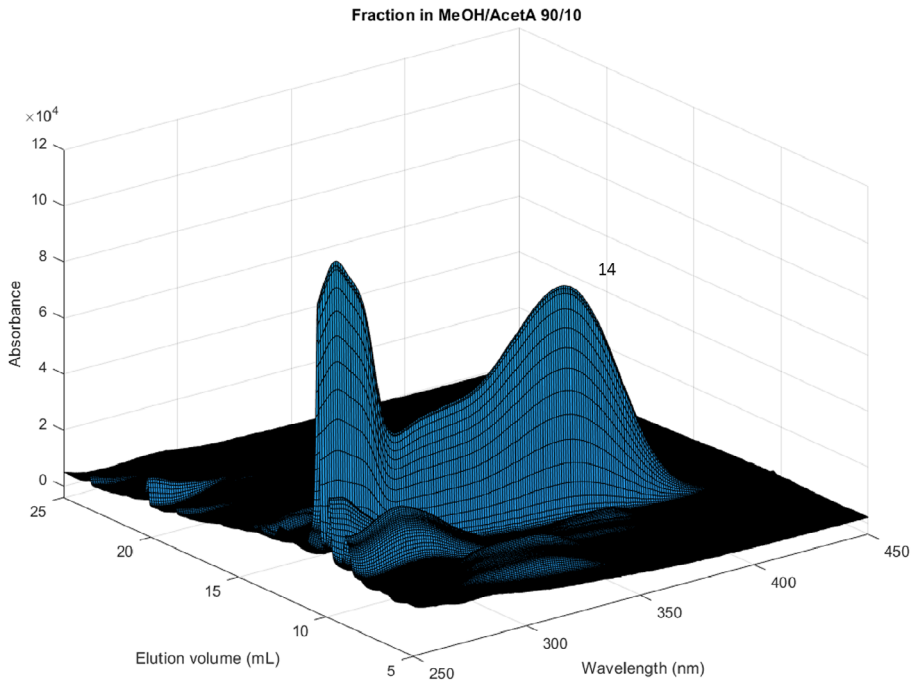

FIGURE 10 3D view for the HPLC-DAD analysis for the fraction desorbed from the pyridyl active MIP hybrid particles at $T = 45°C$ with MeOH/AcetA 90/10 as eluent. The previous sorption step was made at $T = 15°C$ using a diatomaceous earth extract in EtOH/water 80/20 and $C = 3.75$ mg mL^{-1}. The huge enrichment with the flavonol quercetin-o-hexuronoside achieved in this fraction is here highlighted.

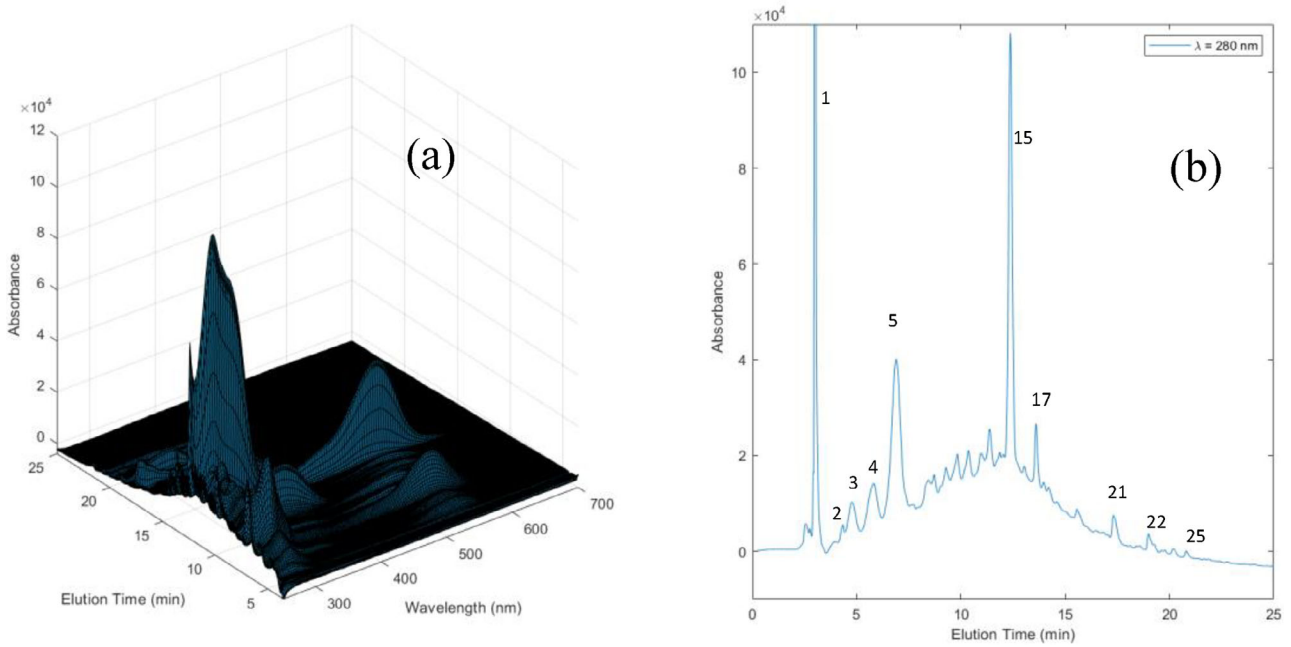

FIGURE 11 3D HPLC-DAD chromatogram (A) and correspondent 2D view at 280 nm (B) for a grape pomace extract used in this work. The following relevant identification for anthocyanin and flavonol compounds in the extract is possible: (5) malvidin 3-O-glucoside (oenin), (15) malvidin-3-O-acetylglucoside (21) quercetin.

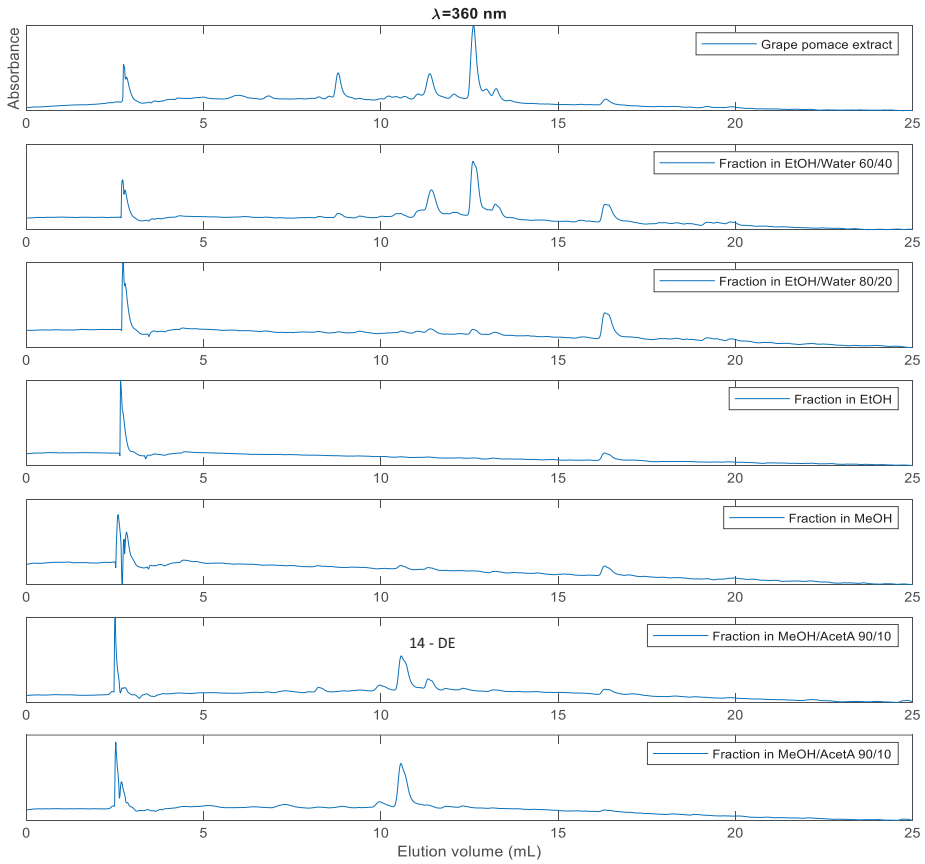

FIGURE 12 HPLC-DAD analyses for different fractions desorbed from the pyridyl active MIP hybrid particles at $T = 45°C$ with diverse solvents as eluents (see inset legend for each fraction). The previous sorption step was made at $T = 15°C$ using a grape pomace extract in EtOH/water 54/46 and $C = 1.1$ mg mL^{-1}. The wavelength $\lambda = 360$ nm was selected to highlight the combined change of flavonols and anthocyanins composition along the different fractions.

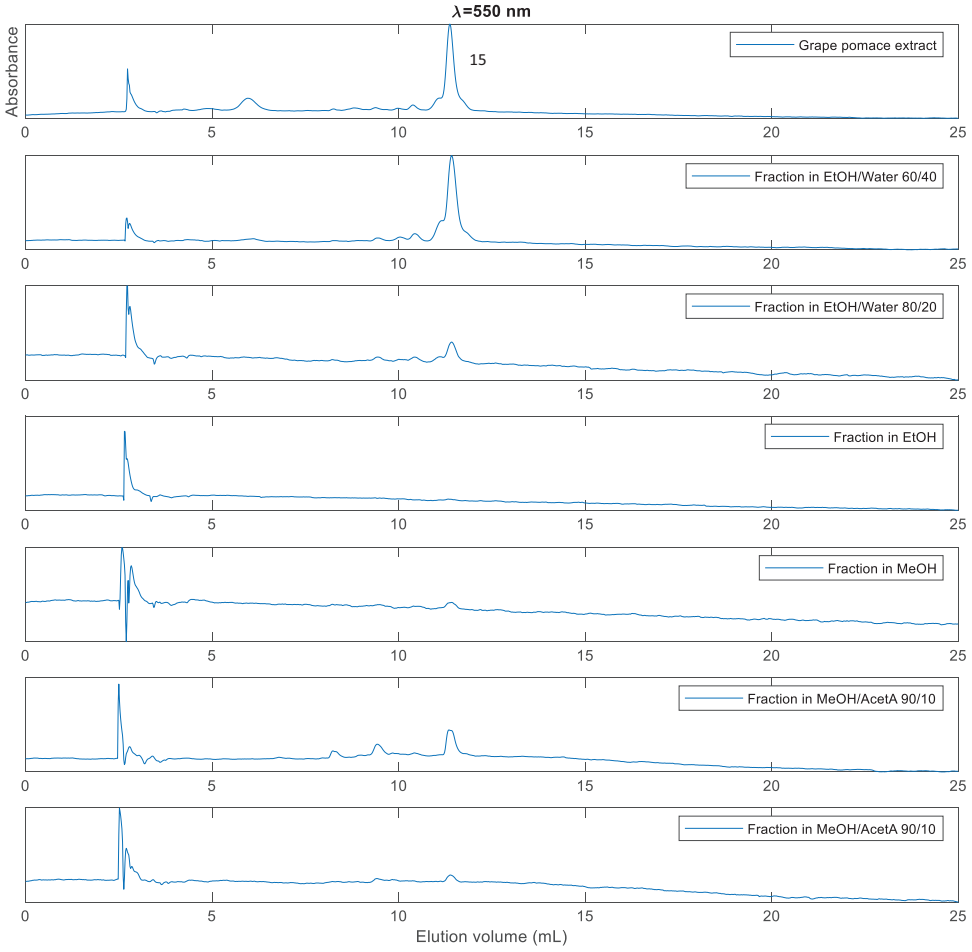

FIGURE 13 HPLC-DAD analyses for different fractions desorbed from the pyridyl active MIP hybrid particles at $T = 45°C$ with diverse solvents as eluents (see inset legend for each fraction). The previous sorption step was made at $T = 15°C$ using a grape pomace extract in EtOH/water 54/46 and $C = 1.1$ mg mL^{-1}. The wavelength $\lambda = 550$ nm was selected to highlight the change of anthocyanins composition along the different fractions.

90/10. Figure 12 compares the HPLC-DAD chromatogram of the initial grape pomace extract with those correspondents to some fractions obtained with this solvent-gradient process. In this comparison, the wavelength $\lambda = 360$ nm was selected to highlight the combined change of flavonols and anthocyanins along the different fractions produced.

These results show that, when compared with the initial grape pomace extract, the fractions with solvent composition up to ethanol/water 60/40 are rich with anthocyanins, specially the abundant malvidin-3-O-acetylglucoside, (peak 15 in Figure 11). The fractions obtained with ethanol/water 80/20, ethanol and methanol are highly enriched with quercetin (the template used for imprinting of hybrid particles surface), while the fractions with methanol/acetic acid 90/10 present a very high content in a molecule potentially matching with quercetin-3-glucuronide, as above analyzed with the diatomaceous earth extract. As before, besides the -OHs groups in quercetin-3-glucuronide, the extra -COOH in this molecule should ground a strong binding with pyridyl basic moieties, leading to its displacement only with a stronger elution solvent, namely with the inclusion of acetic acid. Considering the chromatogram areas at 280 nm, enrichment factors of 4.2 and 8 are estimated for quercetin and quercetin-3-glucuronide, in fractions EtOH/0/20 and 2nd MeOH/AcetA 90/20, respectively.

Figure 13 compares the same HPLC-DAD chromatograms at $\lambda = 550$ nm to highlight the particular change of anthocyanins along the different fractions produced. Note again that their presence is magnified in the first stages of desorption (initial water richer fractions up to ethanol/water 60/40) and minimized in the ethanol/water 80/20, ethanol and methanol fractions. Interestingly, the presence of three well-defined anthocyanins is observed in the first fraction obtained with methanol/acetic acid, showing the importance of acidification for the elution of traces of these compounds still bind to the adsorbent. Globally, results in Figures 12

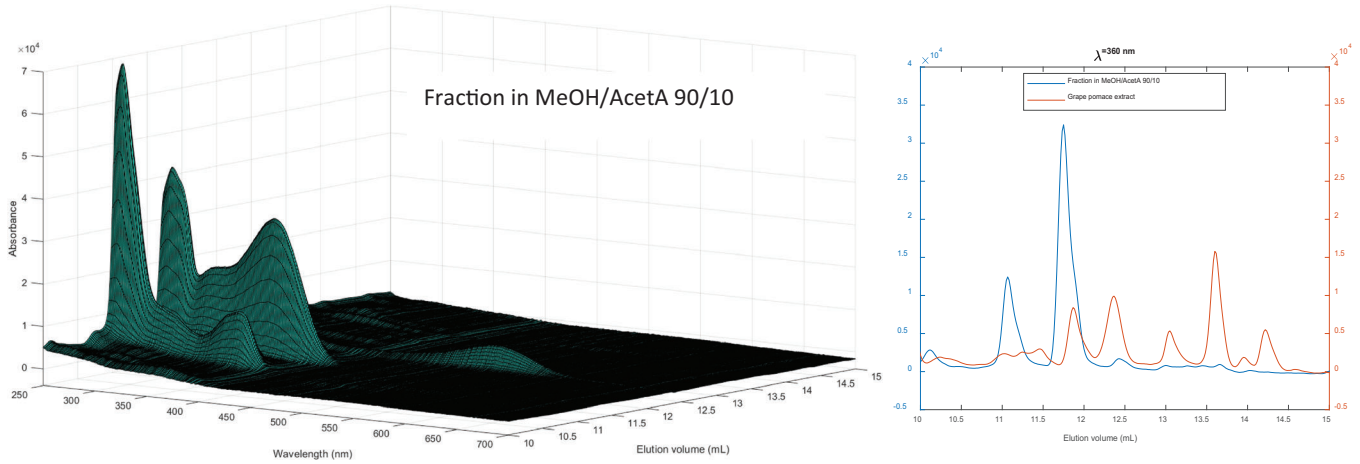

FIGURE 14 HPLC-DAD analysis for a fraction desorbed from the pyridyl active MIP hybrid particles at $T = 45°C$ with MeOH/AcetA 90/10 as eluent. The previous sorption step was made at $T = 20°C$ using a grape pomace extract in EtOH/water 80/20 and $C = 1$ mg mL^{-1}. A fraction enriched with flavonols is here showed.

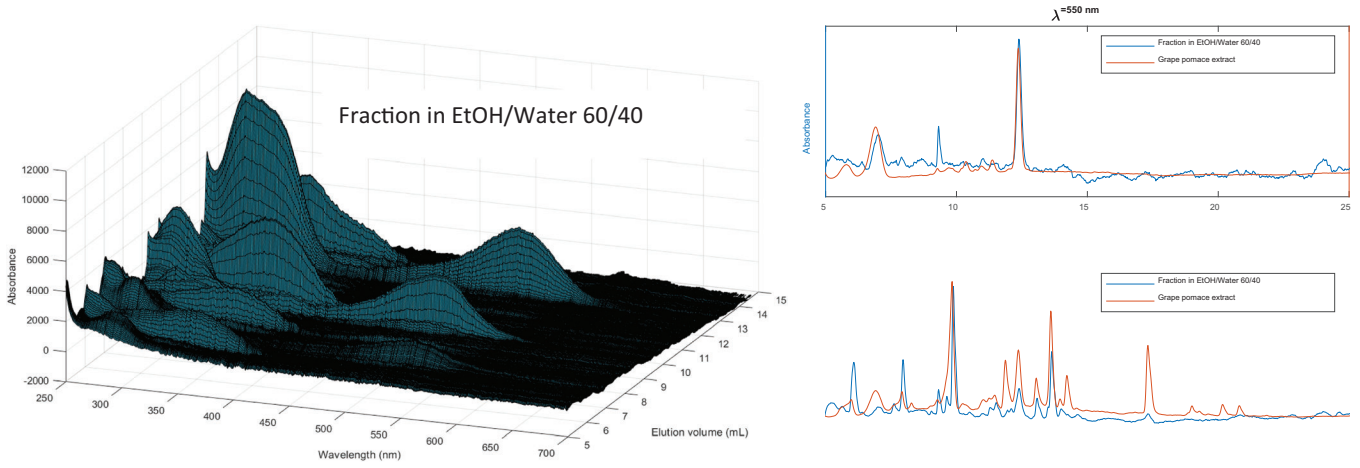

FIGURE 15 HPLC-DAD analysis for a fraction desorbed from the pyridyl active MIP hybrid particles at $T = 45°C$ with EtOH/water 60/40 as eluent. The previous sorption step was made at $T = 20°C$ using a grape pomace extract in EtOH/water 80/20 and $C = 1$ mg mL^{-1}. A fraction enriched with anthocyanins is here showed.

and 13 show the usefulness of the developed adsorbents for the fractionation of flavonols and anthocyanins in grape pomace extracts. Note that a different designing of the temperature-swing/solvent-gradient processes can be considered to achieve an additional tailoring of the composition of the phenolic compounds in the produced fractions.

A different set of operation conditions concerning the grape pomace extract used and loading conditions were considered in other experimental runs and some relevant outcomes are presented in Figures 14 and 15. In this run, the sorption step was made at $T = 20°C$ using a grape pomace extract in EtOH/water 80/20 and $C = 1$ mg mL^{-1}. A different grape pomace extract was here used in order to simulate the likely variability of the starting biomass (changing of the grapes variety, geographical origin, etc.) and the eventual impact in the fractionation process. Results in Figures 14 and 15 highlights again the good performance of the developed hybrid MIP particles with the enrichment of different classes of polyphenols in grape pomace. Specifically, Figure 14 shows a fraction enriched for two flavonols which identification is compatible with myricetin and quercetin glucosides previously found in the diatomaceous earth extract (see previous section). Enrichment factors up to 4 in these flavonols were estimated in the fractions produced. As mentioned above, nonspecific binding of other molecules than the MIP template is unavoidable with such complex mixtures and working with interfering solvents as ethanol/water mixtures. However, the results here presented demonstrate

the usefulness of using quercetin as a kind of surrogate for materials textural improvement and enrichment of other flavonols in the mixture. On the other hand, Figure 15 shows the production of anthocyanins rich fractions when manipulating through sorption/desorption the same extract. Note the lower incidence for flavonols observed for fraction in Figure 15 and the clear presence of anthocyanins such as oenin (malvidin 3-O-glucoside), malvidin-3-O-acetylglucoside and other minority related compounds derived from malvidin, delphidin, cyanidin, petunidin, and peonidin[44] which become apparent in the visible region of the spectrum.

3 | CONCLUSIONS

Hybrid cellulose-synthetic particles with surface active pyridyl groups and molecularly imprinted binding sites generated with quercetin as template were prepared via ATRP. The functionalization of the materials with pyridyl moieties was confirmed and the SEM analysis of the hybrid particles clearly demonstrates their surface modification as compared with the native cellulose. An imprinting factor IF ~8 was estimated through competitive sorption/desorption of a mixture of standard polyphenols quercetin/ferulic acid/rutin in the imprinted and non-imprinted developed particles. Furthermore, a high retention of polyphenols in the hybrid materials was observed even when using hydroalcoholic solvents with high ethanol content (e.g., ethanol/water 80/20 v/v). This important outcome is possible due to the strong binding of polyphenols with the surface active pyridyl moieties.

The particular features of the synthesized materials were scrutinized in view of their use as adsorbents for the efficient fractionation of flavonols and anthocyanins in winemaking residues. Agro-industrial diatomaceous earth and grape pomace residues were used as a source of these bioactive compounds and high concentration and enrichment factors were achieved with the designed sorption/desorption processes. For instance, fractions with enrichment factor 5 for quercetin and 12 for quercetin-3-O-glucuronide were observed with the processing of the diatomaceous earth extract. On the other hand, the production of fractions with separated enrichment of anthocyanins and flavonols was demonstrated for grape pomace extracts. Enrichment factors up to 4 for flavonols (e.g. myricetin and quercetin glucosides) were obtained with grape pomace extracts.

The present work considers the possible addressing of sustainability concerns combining three action lines: i) the incorporation of cellulose in the developed adsorbents, ii) the designing of sorption/desorption methods contributing for process intensification and iii) the valorization of winemaking residues in framework of circular bio-economy. The efficient exploitation of agro-industry generated waste and by-products to obtain high added-value products, namely drugs, nutraceuticals, cosmeceuticals, a working line in the United Nations 2030 Agenda for Sustainable Development, drives the research line here explored.

4 | EXPERIMENTAL SECTION

Materials: All chemicals were used as purchased, without further purification. Microcrystalline cellulose (MCC, powder, 20 μm, cotton linters), BIBB (α-bromoisobutyryl bromide, 98% purity), triethylamine (TEA, 99.5% purity), 4-(dimethylamino)pyridine (DMAP, purity≥ 99%), CuBr (copper(I) bromide, 97% purity), and PMDETA (N′′,N′′-pentamethyldiethylenetriamine, 99% purity) was purchased from Sigma-Aldrich. 4-vinylpyridine (4VP, 95% purity) was provided by Alfa Aesar. Analytical reagent grades for ACN (acetonitrile), DMF (dimethylformamide), acetic acid (AcOH), and methanol (MeOH) were bought from Fisher Scientific and for ethanol (EtOH) from Pan-Reac. Quercetin (hydrate, purity 95%), rutin (purity 97%) and ferulic acid (purity 99%) were supplied by Acros Organics. These standard polyphenols were used in the synthesis and testing of the materials here addressed. The water used in the experiments was ultrapure water supplied by the local laboratory.

Surface Imprinting in MCC-Br Macroinitiator Particles via ATRP: The reaction path considered was previously detailed presented[17] and includes: i) the immobilization of BIBB in MCC, ii) the surface imprinting in MCC-Br macroinitiator particles via ATRP. The first step involves the MCC dispersion in DMF using sonication and then the reaction of BIBB with MCC hydroxyls in the presence of triethylamine and DMAP. The second step includes the dried ATRP macroinitiator MCC-Br produced in step i), the functional monomer 4VP, the template quercetin and the crosslinker EGDMA as well as the ATRP pair CuBr/PMDETA. Ethanol was considered in step ii) for the synthesis of the particles here used and the polymerization took place in a sealed vessel during 72 hours at 70°C.[17]

Products Characterization using FTIR Spectroscopy: Purified and dried MIP was characterized through FTIR spectroscopy with a Perkin Elmer, model Spectrum Two, instrument. These analyses were directly performed in ATR mode and also with the particles mixed with KBr and pressed into pellets in order to collect the correspondent IR spectra.

SEM analysis for the pristine cellulose, MIP and NIP hybrid cellulose-synthetic particles: Scanning Electron Microscopy (SEM) characterization of the particles

involved in this research was performed at the International Iberian Nanotechnology Laboratory (INL), Braga, using the FIB/SEM system HELIOS Nanolab 450S. SEM imaging was obtained using an electron beam of 3 keV, beam current 25 pA and field free lens mode.

Measurement of the surface area and pore volume of the adsorbents: The Brunauer–Emmett–Teller (BET) specific surface area and pore volume of the produced adsorbent particles were determined through N_2 adsorption/desorption isotherms at 77 K using a Quantachrome NOVA 4200e adsorption analyzer.

HPLC-DAD Analysis: An HPLC system (KNAUER) consisting of a gradient pump (P6.1 L) equipped with a degasser, an autosampler (6.1 L), a column thermostat (CT2.1), and a DAD (photodiode-array detector, 6.1 L) was used in this research. ClarityChrom was the software allowing the control of the HPLC system. The chromatographic analysis was performed using an Ascentis C18 (SUPELCO) column with a particle size of 5 μm and dimensions 25 cm × 4.6 mm. A gradient of solvents was used as a mobile phase varying from 100% of water-ACN (9:1) to 100% water-ACN (1:9) for 45 minutes. The mobile phase water pH was adjusted to 3 using acetic acid. The flow rate of the chromatographic analyses was 1 $mLmin^{-1}$, and the temperature of the column was set at 45°C.

Competitive sorption/desorption experiments with polyphenol standards: Assessment of the competitive sorption/desorption capabilities of the MIPs/NIPs was performed with 25 mg of the dry materials in SPE packing cartridges (Agilent Bond Elut reservoir, 1 mL capacity). Adsorbents were first cleaned (successive loading and elution steps using methanol/acetic acid 90/10 with UV/vis monitoring) and afterward conditioned with the desired testing solvent (e.g., ethanol/water 80/20), during at least 24 hours before use. Cartridges were then loaded with 2.5 mL of the mixture of polyphenol standards ferulic acid/rutin/quercetin solution in ethanol/water 80/20 with concentration 0.1 mM for each compound, considering typically 15 minutes for total percolation time. The adsorbed amounts for each polyphenol were quantified through HPLC-DAD analysis of the liquid collected at column outlet. The washing desorption step was performed by percolating the same volume of clean solvent (ethanol/water 80/20) through the adsorbent particles and, afterward, the elution desorption step was made with the same volume of methanol/acetic acid 90/10. Desorbed amounts for each polyphenol were quantified also by HPLC-DAD analysis of the collected liquid phases in the washing and elution desorption steps.

Preparation of diatomaceous earth and grape pomace hydroalcoholic extracts: Diatomaceous earth and grape pomace winemaking by-products were supplied by Caves Campelo S.A. (Portugal) during the harvest season in September 2021. Extraction of phenolic compounds was performed using ethanol/water 80:20 (v/v) as solvent in a ratio 20/1 solvent/solid-residue. Sonication followed by agitation were used as extraction methods. At the end, the supernatants were collected and evaporated under vacuum on a rotary evaporator. The final dry residues were used to prepare solutions at the selected conditions (solvent, concentration) to be used in sorption/desorption runs with the HPLC-packed hybrid MIP particles.

Sorption/desorption experiments with winemaking residues extracts: Hybrid MIP particles (2400 mg) with active pyridyl groups were packed in a HPLC column (L = 125 mm and D = 8 mm) using the slurry method. A Knauer HPLC pump (model Azura P 4. 1S, titanium head) with maximum delivery pressure of 40 MPa and flow rate in the range 0.001 to 10 mL min^{-1} was used to make the flow of the feeding solutions and desorption solvents through the hybrid MIP-packed column (flow-rate = 1 mL min^{-1}). A column oven was used to define the temperature of the sorption/desorption steps and the temperature of the feeding solution or desorption solvents was controlled using a thermostatic bath.

ACKNOWLEDGMENTS

The authors are thankful for the funding through the project "BacchusTech-Integrated Approach for the Valorization of Winemaking Residues" (POCI-01-0247-FEDER-069583), supported by the Competitiveness and Internationalization Operational Program (COMPETE 2020), under the PORTUGAL 2020 Partnership Agreement, through the European Regional Development Fund (ERDF). Catarina Gomes acknowledges to FCT for the PhD scholarship 2020.06057.BD. R.D. is grateful to the Foundation for Science and Technology (FCT, Portugal) for financial support through national funds FCT/MCTES (PIDDAC) to CIMO (UIDB/00690/2020 and UIDP/00690/2020) and SusTEC (LA/P/0007/2020). M.R.C. acknowledges the support by LA/P/0045/2020 (ALiCE), UIDB/50020/2020, and UIDP/50020/2020 (LSRE-LCM), funded by national funds through FCT/MCTES (PIDDAC).

CONFLICT OF INTEREST STATEMENT

The authors declare that they have no known competing financial interests or personal relationships that could have appeared to influence the work reported in this paper.

DATA AVAILABILITY STATEMENT

The data that support the findings of this study are available from the corresponding author upon reasonable request.

ORCID

Rolando C. S. Dias https://orcid.org/0000-0001-7369-382X

REFERENCES

1. S. Varshney, N. Mishra, Pyridine-based polymers and derivatives: synthesis and applications. In *Recent Developments in the Synthesis and Applications of Pyridines*. (Editor(s): Parvesh Singh) **2023**, 43–69. Chapter 2. Elsevier ISBN 9780323912211. https://doi.org/10.1016/B978-0-323-91221-1.00012-9
2. Y. N. Chen, W. Zhao, J. C. Zhang, *RSC Adv.* **2017**, *7*, 4226. https://doi.org/10.1039/C6RA26813G
3. E. S. Yanovska, L. O. Vretik, O. A. Nikolaeva, Y. Polonska, D. Sternik, O. Y. Kichkiruk, *Nanoscale Res. Lett.* **2017**, *12*, 217. https://doi.org/10.1186/s11671-017-1991-2
4. C. M. Xiao, J. M. Lin, *ACS Omega* **2020**, *5*, 23099. https://doi.org/10.1021/acsomega.0c02874
5. Y. A. B. Neolaka, Y. Lawa, J. N. Naat, A. A. P. Riwu, H. Darmokoesoemo, G. Supriyanto, C. I. Holdsworth, A. N. Amenaghawon, H. S. Kusuma, *React. Funct. Polym.* **2020**, *147*, 104451. https://doi.org/10.1016/j.reactfunctpolym.2019.104451
6. N. Amaly, Y. Ma, A. Y. El-Moghazy, G. Sun, *Sep. Purif. Technol.* **2020**, *250*, 117086. https://doi.org/10.1016/j.seppur.2020.117086
7. M. Atif, C. S. Chen, M. Irfan, F. Mumtaz, K. He, M. Zhang, L. J. Chen, Y. M. Wang, *Eur. Polym. J.* **2019**, *120*, 109199. https://doi.org/10.1016/j.eurpolymj.2019.08.026
8. N. Sahiner, O. Ozay, *React. Funct. Polym.* **2011**, *71*, 607. https://doi.org/10.1016/j.reactfunctpolym.2011.03.003
9. M. Chanda, K. F. O'Driscoll, G. L. Rempel, *Reactive Polymers, Ion Exchangers, Sorbents* **1983**, *1*, 281. https://doi.org/10.1016/0167-6989(83)90031-4.
10. H. El-Hamshary, S El-Sigeny, M. F. A. Taleb, N. A. El-Kelesh, *Sep. Purif. Technol.* **2007**, *57*, 329. https://doi.org/10.1016/j.seppur.2007.04.013
11. N. Fontanals, P. Puig, M. Galià, R. M. Marcé, F. Borrull, *J. Chromatogr. A* **2004**, *1035*, 281. https://doi.org/10.1016/j.chroma.2004.02.049
12. A. Bzainia, R. C. S. Dias, M. R. P. F. N. Costa, *Macromol. React. Eng.* **2023**, *2200076*, 1. https://doi.org/10.1002/mren.202200076
13. C.P. Gomes, G. Sadoyan, R. C. S. Dias, M. R. P. F. N. Costa, *Processes* **2017**, *5*, 1. https://doi.org/10.3390/pr5040072
14. C. P. Gomes, R. C. S. Dias, M. R. P. F. N. Costa, *Chromatographia* **2019**, *82*, 893. https://doi.org/10.1007/s10337-019-03728-7
15. C. P. Gomes, V. Franco, R. C. S. Dias, M. R. P. F. N. Costa, *Chromatographia* **2020**, *83*, 1539. https://doi.org/10.1007/s10337-020-03958-0
16. A. Bzainia, R. C. S. Dias, M. R. P. F. N. Costa, *Molecules* **2022**, *27*, 6406. https://doi.org/10.3390/molecules27196406
17. C. P. Gomes, R. C. S. Dias, M. R. P. F. N. Costa, *Macromol. React. Eng.* **2023**, *17*, 2300011. https://doi.org/10.1002/mren.202300011
18. C. P. Gomes, R. C. S. Dias, M. R. P. F. N. Costa, *React. Funct. Polym.* **2021**, *164*, 104930. https://doi.org/10.1016/j.reactfunctpolym.2021.104930
19. J. Zuo, P. Ma, Z. Li, Y. Zhang, D. Xiao, H. Wu, A. Dong, *Macromol. Mater. Eng.* **2023**, *308*, 2200499. https://doi.org/10.1002/mame.202200499
20. V. D. Salian, M. E. Byrne, *Macromol. Mater. Eng.* **2013**, *298*, 379. https://doi.org/10.1002/mame.201200191
21. X. Ding, P. A. Heiden, *Macromol. Mater. Eng.* **2014**, *299*, 268. https://doi.org/10.1002/mame.201300160
22. H. Mittal, S. S. Ray, S. S. M. Okamoto, *Macromol. Mater. Eng.* **2016**, *301*, 496. https://doi.org/10.1002/mame.201500399
23. C. R. Reddy, L. C. Simon, *Macromol. Mater. Eng.* **2010**, *295*, 906. https://doi.org/10.1002/mame.201000210
24. A. Gebrekrstos, J. T. Orasugh, T. S. Muzata, S. S. Ray, *Macromol. Mater. Eng.* **2022**, *307*, 2200185. https://doi.org/10.1002/mame.202200185
25. W. Chen, B. Sun, P. Biehl, K. Zhang, *Macromol. Mater. Eng.* **2022**, *307*, 2200072. https://doi.org/10.1002/mame.202200072
26. M.P. Vocht, P. Tomasic, R. Beyer, A. Müller, U. Zuberbühler, B. Stürmer, F. Hermanutz, M. R. Buchmeiser, *Macromol. Mater. Eng.* **2022**, *307*, 2200093. https://doi.org/10.1002/mame.202200093
27. Z. Tang, S. Bian, Z. Lin, H. Xiao, M. Zhang, K. Liu, X. Li, B. Du, L. Huang, L. Chen, Y. Ni, H. Wu, *Macromol. Mater. Eng.* **2021**, *306*, 2100232. https://doi.org/10.1002/mame.202100232
28. K. Müller, C. Zollfrank, M. Schmid, *Macromol. Mater. Eng.* **2019**, *304*, 1800760. https://doi.org/10.1002/mame.201800760
29. N. Gour, K. X. Ngo, C. Vebert-Nardin, *Macromol. Mater. Eng.* **2014**, *299*, 648. https://doi.org/10.1002/mame.201300285
30. M. Arabi, A. Ostovan, J. Li, X. Wang, Z. Zhang, J. Choo, L. Chen, *Adv. Mater.* **2021**, *33*, 2100543. https://doi.org/10.1002/adma.202100543
31. A. Ostovan, M. Arabi, Y. Wang, J. Li, B. Li, X. Wang, L. Chen, *Adv. Mater.* **2022**, *34*, 2203154. https://doi.org/10.1002/adma.202203154
32. M. M. Contreras, J. M. Romero-García, J. C. López-Linares, I. Romero, E. Castro, *Food Bioproducts Processing* **2022**, *134*, 56. https://doi.org/10.1016/j.fbp.2022.05.005
33. T. Atatoprak, M. M. Amorim, T. Ribeiro, M. Pintado, A. R. Madureira, *Food Chem.: Mol. Sci.* **2022**, *4*, 100067, https://doi.org/10.1016/j.fochms.2021.100067
34. A. Carlmark, E.E. Malmström, *Biomacromolecules* **2003**, *4*, 1740. https://doi.org/10.1021/bm030046v
35. X. Sui, J. Yuan, M. Zhou, J. Zhang, H. Yang, W. Yuan, Y. Wei, C. Pan, *Biomacromolecules* **2008**, *9*(10), 2615. https://doi.org/10.1021/bm800538d
36. Z. Zhang, X. Wang, K. C. Tam, G. Sèbe, *Carbohydr Polym* **2019**, *205*, 322. https://doi.org/10.1016/j.carbpol.2018.10.050
37. Z. Zhang, K. C. Tam, G. Sèbe, X. Wang, *Carbohydr. Polym.* **2018**, *199*, 603. https://doi.org/10.1016/j.carbpol.2018.07.060
38. L. Wu, U. Glebe, A. Böker, *Macromolecules* **2016**, *49*, 9586. https://doi.org/10.1021/acs.macromol.6b01792
39. Y. Yin, X. Tian, X. Jiang, H. Wang, W. Gao, *Carbohydr. Polym.* **2016**, *142*, 206. https://doi.org/10.1016/j.carbpol.2016.01.014
40. J. Cao, C. Shen, X. Wang, Y. Zhu, S Bao, X Wu, Y. Fu, *Carbohydr. Polym.* **2021**, *251*, 117026. https://doi.org/10.1016/j.carbpol.2020.117026
41. P. Pérez-Larrán, B. Díaz-Reinoso, A. Moure, J. L. Alonso, H. Domínguez, *Curr. Opin. Food Sci.* **2018**, *23*, 165. https://doi.org/10.1016/j.cofs.2017.10.005
42. I. Drevelegka, A. M. Goula, *Chem Eng Process* **2020**, *149*, 107845. https://doi.org/10.1016/j.cep.2020.107845
43. S. Heravi, M. Rahimi, M. Shahriari, S. N. Ebrahimi, *Chem. Eng. Res. Des.* **2022**, *183*, 382. https://doi.org/10.1016/j.cherd.2022.05.011
44. C. N. Duarte, O. Taofiq, M. I. Dias, S. A. Heleno, C. Santos-Buelga, L. Barros, J. S. Amaral, *Cosmetics* **2023**, *10*, 58, https://doi.org/10.3390/cosmetics10020058

45. E. Cioffi, L. Comune, S. Piccolella, M. Buono, S. Pacifico, *Foods* **2023**, *12*, 2646. https://doi.org/10.3390/foods12142646
46. A. Panche, A. Diwan, S. Chandra, *J Nutr Sci* **2016**, *5*, E47. https://doi.org/10.1017/jns.2016.41
47. M. S. S. Chagas, M. D. Behrens, C. J. Moragas-Tellis, G. X. M. Penedo, A. R. Silva, C. F. Gonçalves-de-Albuquerque, *Oxid. Med. Cell. Longevity* **2022**, *2022*, Article ID 9966750. https://doi.org/10.1155/2022/9966750
48. S. Habtemariam, Editor(s): S. Habtemariam, *Medicinal Foods as Potential Therapies for Type-2 Diabetes and Associated Diseases*, Academic Press, **2019**, 135–175, https://doi.org/10.1016/B978-0-08-102922-0.00007-9
49. F. He, L. Mu, G.-L. Yan, N.-N. Liang, Q.-H. Pan, J. Wang, M. J. Reeves, C.-Q. Duan, *Molecules* **2010**, *15*, 9057. https://doi.org/10.3390/molecules15129057
50. I. B. Coutinho, A. Freitas, A. L. Maçanita, J. C. Lima, *Food Chem.* **2015**, *172*, 476. https://doi.org/10.1016/j.foodchem.2014.09.060

SUPPORTING INFORMATION

Additional supporting information can be found online in the Supporting Information section at the end of this article.

How to cite this article: C. P. Gomes, R. C. S. Dias, M. R. P. F. N. Costa, *Nano Select* **2024**, e2300153. https://doi.org/10.1002/nano.202300153